

Topography of the Lunar Poles from Radar Interferometry: A Survey of Cold Trap Locations

J. L. Margot,^{1*}† D. B. Campbell,^{1†} R. F. Jurgens,² M. A. Slade²

Detailed topographic maps of the lunar poles have been obtained by Earth-based radar interferometry with the 3.5-centimeter wavelength Goldstone Solar System Radar. The interferometer provided maps 300 kilometers by 1000 kilometers of both polar regions at 150-meter spatial resolution and 50-meter height resolution. Using ray tracing, these digital elevation models were used to locate regions that are in permanent shadow from solar illumination and may harbor ice deposits. Estimates of the total extent of shadowed areas poleward of 87.5 degrees latitude are 1030 and 2550 square kilometers for the north and south poles, respectively.

Topographic depressions near the lunar poles provide a low-temperature environment that is a potential reservoir of water ice deposits (1, 2). The case for lunar ice was recently strengthened by the detection of a hydrogen signature near the polar regions by the neutron spectrometer aboard the Lunar Prospector (LP) spacecraft (3). However, it is still unknown whether the excess hydrogen measured by LP correlates with regions where the thermal conditions are compatible with the presence of water ice. Here, radar-derived topographic maps of the lunar poles are used to locate shadowed regions that may act as cold traps for ice deposits.

Studies of the behavior of volatiles on the moon have suggested that water ice deposits might survive for billions of years in cold traps near the lunar poles (1, 2). The possible source mechanisms for that water include cometary and meteoroidal impacts, reduction of FeO by hydrogen derived from the solar wind, and degassing of the interior (1, 2). Water molecules liberated on the moon assume ballistic trajectories (1, 2, 4) until they are destroyed in flight or trapped in low-temperature regions (5). Ice on the lunar surface is subject to destructive processes, including solar photon-induced desorption (2, 6), erosion by sputtering (2, 6, 7), and photodissociation by interstellar hydrogen Lyman- α radiation (6). These surface loss processes imply that any ice deposits would have to be protected by a thin regolith layer.

The first attempts to provide observational

evidence of lunar ice deposits used radar techniques (8, 9). Icy bodies in the solar system exhibit abnormal radar signatures, high backscatter cross sections, and a ratio of same sense-to-opposite sense circular polarization that is larger than unity. These characteristics have been observed unambiguously in Earth-based radar echoes from permanently shadowed craters near the poles of Mercury (10), but the lunar observations were much less conclusive. A study of Clementine radar data resulted in a report of a possible detection of water ice on the moon (8), but a separate analysis of the same data did not find a distinctive ice signature (11). Earth-based radar observations of the lunar poles did not show evidence of ice deposits (9).

Because the lunar poles have never been observed over the entire possible range of solar illumination conditions (12), establishing the correlation between the hydrogen signature detected by LP (3) and the locations of terrain in permanent shadow has been difficult. We used Earth-based radar interferometry to obtain topographic maps of the lunar polar regions at 150-m spatial and 50-m height resolutions. These digital elevation models (DEMs) were used to simulate solar illumination conditions to determine the locations of the lunar cold traps, which are possible reservoirs of water ice. Unlike previous estimates of the extent of shadowed areas at the lunar poles (8, 13), this survey took into account the entire solar illumination cycle.

Detailed topographic maps of the lunar surface can be acquired with an Earth-based radar interferometer (14, 15). The measurements rely on range differences between points on the lunar surface and two receivers located on Earth. Changes in elevation are observable because they affect the relative phase between the two radar echoes (14).

The antennas of the Deep Space Network (DSN) at Goldstone, California, were used to

observe the lunar poles in October 1997. The 70-m parabolic dish was used to transmit a pulsed binary-coded waveform at a wavelength of 3.5 cm; two 34-m antennas separated by 20 km formed the receiving interferometer. Separate maps of the (complex) radar backscatter were produced from each receiving site by means of the conventional delay-Doppler technique (16). The interferometric phase was then extracted on a per pixel basis and translated to topographic changes.

The viewing geometry at the time of our observations was such that the radar line of sight rose 6° to 7° above the horizon at the lunar poles, which is close to the maximum allowed by the Earth-moon geometry. At these angles, a fraction of the lunar landscape in the field of view was not illuminated by the radar because of shadowing effects. It was not possible to determine the altitudes of these areas of radar shadow.

We verified the validity and accuracy of the elevation maps by comparing our radar-derived topography to Clementine laser altimetry measurements at latitudes between 70° and 80° (17). This comparison, yielding ~100-m root mean square deviations between the two techniques, provided absolute height references and also permitted the removal of small residual slopes from our DEMs. Slope corrections of 0.07° and 0.1° were applied to the north and south pole DEMs, respectively.

Given a model for the topography of the lunar poles, the problem of finding regions of permanent shadow becomes purely geometric, because the Earth-moon orbital parameters and the orientation of the moon's spin axis are known. Because the orientation of the lunar spin vector is fixed with respect to the ecliptic, the limb of the sun rises a maximum of 1.85° above the horizon at the lunar poles. Although the moon's axial tilt may have had large variations in the past, it is thought to have been in its present configuration for the past ~2 billion years (18). We implemented a ray-tracing procedure that simulates solar illumination conditions in the polar regions, with the finite angular size of the sun and latitudinal effects taken into account (19). Points that are surrounded by topography that blocks sunlight at all times were marked as permanently shadowed terrain. All other areas were marked as illuminated terrain, except for regions of unknown topography, which were left undefined (20).

Because illumination conditions in regions of radar shadow, and hence unknown topography, could not be determined by the ray-tracing procedure, we visually inspected the illumination map and marked additional regions that are believed to lie in permanent shadow. This extrapolation was performed only for craters that contained radar-shadowed terrain adjacent to sun-shadowed ter-

¹Department of Astronomy, Space Sciences Building, Cornell University, Ithaca, NY 14853, USA. ²Jet Propulsion Laboratory, MS 238-420, 4800 Oak Grove Drive, Pasadena, CA 91109, USA.

*Present address: Arecibo Observatory, HC3 Box 53995, Arecibo, PR 00612, Puerto Rico.

†To whom correspondence should be addressed. E-mail: margot@naic.edu (J.L.M.); campbell@astro.sun.tn.cornell.edu (D.B.C.)

REPORTS

rain and only when crater rim heights were roughly uniform. Such regions are accounted for separately in the calculation of areal coverage of terrain in permanent shadow.

Topographic maps of the lunar polar regions (Figs. 1 and 2) show that the north polar area displays relatively little topographic expression, whereas the south polar region presents much more rugged terrain. The range of elevations characterizing the south polar region is roughly 2.5 times that at the north.

The extent of permanent shadow was estimated at both poles for rectangular areas approximately encompassing the 85° latitude line (Fig. 3). The amount of permanent shadow for a region 375 km by 225 km centered on the north pole is 2650 km², which is about half the 5100 km² area estimated for a region 325 km by 285 km at the south pole (Table 1).

For the north polar area, shadowed regions are concentrated at the bottom of large craters, forming a crescent in the wall and floor areas that are furthest from the pole. This is observed for Hermite (86.0°N, 270°E) and two other craters (at 85.0°N, 63°E and 85.9°N, 115°E). For high-latitude craters, this shadowing is consistent with a source of illumination that remains almost parallel to the equatorial plane. The characteristic crescent-shaped shadowed region is similar to the appearance of a region of strong radar return

observed for a large polar crater on Mercury (21). Several small lunar craters on the floor of Peary (88.6°N, 33°E) and three larger craters aligned roughly along the 315° longitude line are also protected from sunlight. These five regions constitute the largest potential deposits at the north pole and would be expected to display an excess of hydrogen in neutron flux data (3) if they contained ice. Many small shadowed areas in a region of complex topography between 160° and 300° of longitude are unlikely to meet the thermal requirements for long-term stability of ice, because scattered and emitted thermal energy from surrounding terrain would be significant in this environment.

At the south pole, virtually all of the floors of three craters with diameters in the 39- to 51-km range appear to be in shadow: crater Faustini (87.3°S, 77°E), and craters at 88.1°S, 45°E and 87.5°S, 356°E. There is a high probability, based on measurement and modeling, that the south pole crater Shackleton (89.7°S, 110°E) and a crater at 88.5°S, 273°E have shadowed floors and hence are also cold

traps. Cabeus (85.5°S, 45°E) contains additional regions of permanent shadow, although their outlines cannot be specified because they are dependent on the unknown height of the northern part of the floor. There are potential cold traps in several other areas, but the large topographical variations in the south polar region mean that extensive areas are in radar shadow, making it difficult to determine whether they are also in permanent solar shadow.

Earth-based radar interferometry can provide topographic maps of the moon with ~150 m horizontal spacing or less and ~50 m height resolution. However, parts of the moon that are never visible from Earth or are in radar shadow cannot be measured. Compared to the quasi-global Clementine laser altimetry data set (17), the radar DEMs offer a factor of 10⁴ increase in the number of elevation points per unit of area. The detailed topography afforded by the radar has applications in cratering studies and, if used in combination with high-resolution gravity models, can provide insights about lunar internal structure. The radar measurements complement existing topographic data sets of the moon by providing absolute elevation levels over the polar regions. They can be used to refine global models of lunar topog-

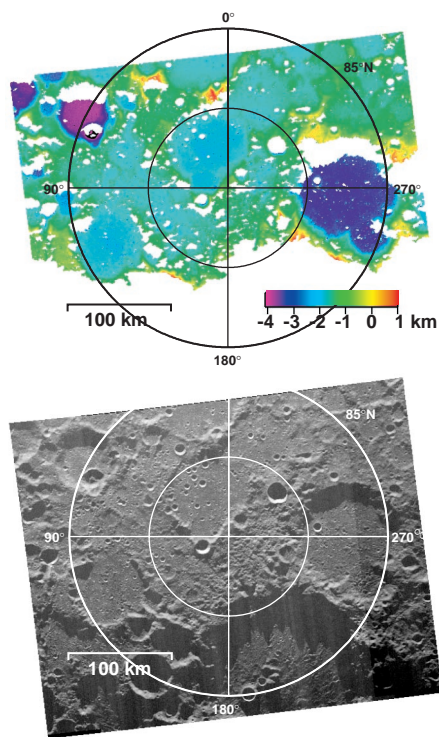


Fig. 1. Digital elevation model (top) and radar backscatter map (bottom) of the north polar region. Absolute elevations with respect to a sphere with a radius of 1738 km are shown. Maps are stereographic projections and use east longitudes.

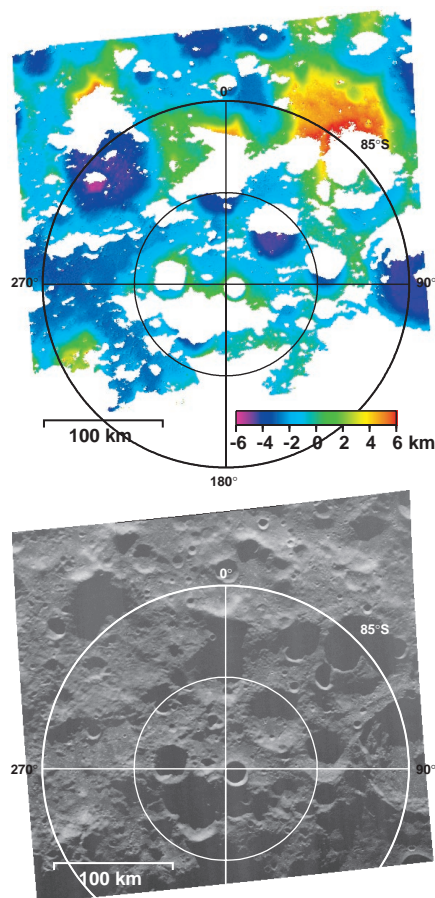


Fig. 2. Digital elevation model (top) and radar backscatter map (bottom) of the south polar region. Absolute elevations with respect to a sphere with a radius of 1738 km are shown. Maps are stereographic projections and use east longitudes.

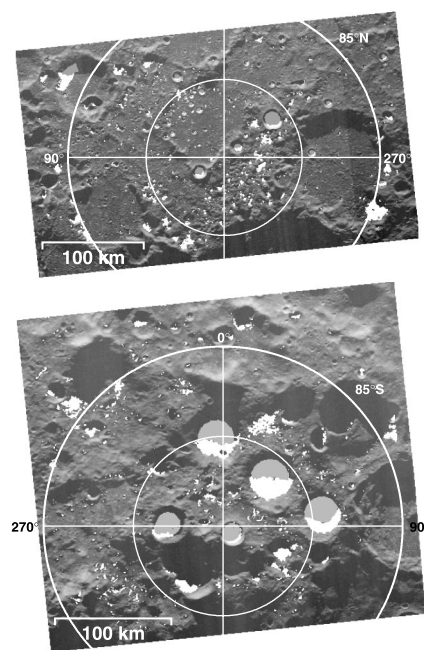


Fig. 3. Locations of cold traps at the lunar north (top) and south (bottom) poles. Areas that were visible to the radar and are in permanent shadow from solar illumination have been marked with white pixel values. Several other regions, which were not visible to the radar (that is, in radar shadow), have been depicted with gray pixels to indicate that they are predicted, on the basis of the topography of the surrounding terrain, to also be in permanent shadow.

Table 1. Extent of areas in permanent shadow at the north and south poles. Surface areas were measured for cold traps that were visible to the radar and were estimated on the basis of modeling for regions that were not visible to the radar. Estimates for regions within 2.5° of the pole are given for comparison with Clementine results (8).

	Measured (km ²)	Estimated (km ²)	Total (km ²)
North pole, imaged area	2080	570	2650
South pole, imaged area	3150	1950	5100
North pole, latitude ≥87.5°	690	340	1030
South pole, latitude ≥87.5° (23)	1480	1070	2550

graphy (17), which currently rely on interpolation over the polar areas. Here we are discussing the use of the radar DEMs to locate cold traps that may harbor ice deposits.

Areas of permanent shadow near the lunar poles occur mostly in crater floors and, at lower latitudes, in crescent-shaped regions on the equatorward, interior areas of crater walls and floors. Several regions of permanent shadow are located at least 5° from the pole, and it is conceivable that shadowed regions could be found at lower latitudes. The existence of permanent shadow in large craters 2° or more from the poles is not in agreement with the results of Zuber and Smith (22), who considered only crater centers in their analysis.

Nozette *et al.* (8) examined illumination conditions within 2.5° of the lunar poles using Clementine images and estimated that 530 km² around the north pole and at least 6361 km² around the south pole were not illuminated by the sun. Our estimates for the north and south poles are 1030 km² and 2550 km², respectively (Table 1), with an upper bound of 4000 km² for the south pole (23). The difference at the north pole may be due to the fact that our simulations delineate many small shadowed areas in the complex region between 160° and 300° of longitude. The large discrepancy in estimates for the south pole is undoubtedly due to the fact that many regions that are in shadow on Clementine images are not in permanent shadow. Clementine observed the moon during southern hemisphere winter, when the south polar region was poorly illuminated. The lighting conditions would have been markedly different during southern hemisphere summer.

The larger amount of shadow at the south pole than at the north pole is potentially inconsistent with the higher hydrogen abundances at the north pole reported by Feldman *et al.* (3) on the basis of LP data. If all cold traps at the lunar poles are equally likely to harbor ice deposits, then the discrepancy with LP neutron data may imply that some of the hydrogen at the poles is not in the form of water ice. Alternatively, ice deposits at the north and south poles may exhibit different signatures in the LP data as a result of different impact histories or differences in burial depths.

The LP neutron energy spectra for the polar regions were interpreted in (3) as being consistent with pure water ice deposits, possibly up to 1.6 m thick, buried under a 40-cm regolith layer. Such meter-thick deposits of clean ice at shallow depths would be expected to manifest themselves in radar returns, but no convincing ice signature was found in either our data or in earlier Arecibo data (9). Several regions of permanent shadow are clearly visible with an Earth-based radar (Fig. 3). Moreover, the penetration depth of the radar waves would be ~30 cm and ~1 m at the 3.5-cm and 12.6-cm wavelengths of the Goldstone and Arecibo instruments, respectively (24). Ice at depths greater than 1 m may not be detectable by either the radar or the LP neutron spectrometer. A few options can be examined in an attempt to reconcile the radar and LP observations: (i) all of the ice deposits happen to be located in regions not visible from Earth, a coincidence that appears unlikely; (ii) the deposits are ice mixed in with regolith or crystals of ice dispersed through the regolith, in which case they would not be observable by radar techniques; (iii) the deposits contain thin alternating layers of relatively pure ice and regolith representing different episodes of deposition (6). Feldman *et al.* (3) indicate that their model of pure ice overlain with regolith is not unique, opening the possibility that models such as (ii) and (iii) may also be consistent with LP data.

References and Notes

1. K. Watson, B. C. Murray, H. Brown, *J. Geophys. Res.* **66**, 3033 (1961).
2. J. R. Arnold, *ibid.* **84**, 5659 (1979).
3. W. C. Feldman *et al.*, *Science* **281**, 1496 (1998).
4. R. R. Hodges Jr., *Proc. Lunar Planet. Sci. Conf.* **11**, 2463 (1980); B. J. Butler, *J. Geophys. Res.* **102**, 19283 (1997).
5. A. P. Ingersoll, T. Svitek, B. C. Murray, *Icarus* **100**, 40 (1992); J. R. Salvail and F. P. Fanale, *ibid.* **111**, 441 (1994); A. R. Vasavada, D. A. Paige, S. E. Wood, in preparation.
6. T. H. Morgan and D. E. Shemansky, *J. Geophys. Res.* **96**, 1351 (1991).
7. L. J. Lanzerotti, W. L. Brown, R. E. Johnson, *ibid.* **86**, 3949 (1981).
8. S. Nozette *et al.*, *Science* **274**, 1495 (1996).
9. N. J. S. Stacy, D. B. Campbell, P. G. Ford, *ibid.* **276**, 1527 (1997).

10. M. A. Slade, B. J. Butler, D. O. Muhleman, *ibid.* **258**, 635 (1992); J. K. Harmon and M. A. Slade, *ibid.*, p. 640; B. J. Butler, D. O. Muhleman, M. A. Slade, *J. Geophys. Res.* **98**, 15003 (1993); J. K. Harmon *et al.*, *Nature* **369**, 213 (1994).
11. R. A. Simpson and G. L. Tyler, *J. Geophys. Res.* **104**, 3845 (1999).
12. The selenographic latitude of the sun oscillates between ±1.6°, with a period roughly equal to 95% of a terrestrial year. By collecting data during about one-sixth of this illumination cycle, the Clementine spacecraft provided the longest continuous observations of the lunar poles by an optical wavelength imaging system.
13. E. M. Shoemaker, M. S. Robinson, E. M. Eliason, *Science* **266**, 1851 (1994).
14. I. I. Shapiro, S. H. Zisk, A. E. E. Rogers, M. A. Slade, T. W. Thompson, *ibid.* **178**, 939 (1972).
15. J. L. Margot, D. B. Campbell, R. F. Jurgens, M. A. Slade, *J. Geophys. Res.*, in press.
16. J. V. Evans and T. Hagfors, Eds., *Radar Astronomy* (McGraw-Hill, New York, 1968).
17. D. E. Smith, M. T. Zuber, G. A. Neumann, F. G. Lemoine, *J. Geophys. Res.* **102**, 1591 (1997). The Clementine laser altimeter returned spot elevations for latitudes below ~80°, with an along-track spacing varying between a few kilometers and a few tens of kilometers. The across-track spacing was ~2.7° longitude, or ~80 km at the equator. Radial errors for the laser measurements are estimated at ~100 m.
18. W. R. Ward, *Science* **189**, 377 (1975).
19. The radar pole positions agree with the Clementine positions to 0.2° of latitude. A 0.2° shift in the latitude of the pole position has a negligible effect on our results.
20. In order to reduce computing time, the ray-tracing procedure sampled azimuth directions with 10° increments, and radial positions along each ray were sampled every kilometer. A 9-by-9 median filter was applied to the resulting illumination maps, effectively removing shadowed regions smaller than 1 km².
21. J. K. Harmon, P. S. Perillot, M. A. Slade, in preparation.
22. M. T. Zuber and D. E. Smith, *Geophys. Res. Lett.* **24**, 2183 (1997).
23. Only two-thirds of the area poleward of 87.5°S was visible to the Goldstone radar, and additional regions near the south pole may contain shadowed terrain. However, Clementine imagery (25) reveals that several regions hidden from the radar are illuminated by the sun. The extent of these illuminated regions gives an upper bound of 1500 km² on the area of any additional cold traps within 2.5° of the pole.
24. The penetration depth L_e is the distance over which the power of an incident wave will be attenuated by a factor e^{-1} . For a low-loss material such as the lunar regolith, it is given by $L_e = \lambda / (2\pi \sqrt{\epsilon} \tan \Delta)$, where ϵ is the dielectric constant and $\tan \Delta$ is the loss tangent. At centimetric and decimetric wavelengths, the moon's regolith can be characterized by a dielectric constant near 2.8 and an effective loss tangent on the order of 0.01, which includes absorptive losses and additional scattering losses. Therefore, the penetration depth is roughly equivalent to 10 wavelengths. Because of refraction at the vacuum-regolith interface, the vertical penetration depth is only weakly dependent on the incidence angle, and even at the poles it would be close to 1 m at 12.6-cm wavelength.
25. S. Nozette *et al.*, *Science* **266**, 1835 (1994).
26. J.L.M. and D.B.C. were partially supported under NASA grant NAG 5-4220 and by the National Astronomy and Ionosphere Center, which is operated by Cornell University under a cooperative agreement with NSF with support from NASA. Part of this work was supported by the Jet Propulsion Laboratory, operated by the California Institute of Technology under contract with NASA. We are grateful to R. Goldstein, H. Zebker, and C. Werner; F. Djuth and J. Elder; the Navigation and Ancillary Information Facility; M. Standish; L. Bracamonte; C. Franck; and R. Winkler, P. Dendrenos, R. Rose, D. Choate, D. Kelley, J. Garnica, G. Bury, G. Farner, R. Littlefair, and C. Snedeker.

20 January 1999; accepted 3 May 1999